

Quantifying Degradation Parameters of Single-Crystalline Ni-Rich Cathodes in Lithium-Ion Batteries

Wengao Zhao*, Kuan Wang, Xinming Fan*, Fucheng Ren, Xieyu Xu, Yangyang Liu, Shizhao Xiong, Xiangsi Liu, Zhengfeng Zhang, Mayan Si, Ruizhuo Zhang, Wessel van den Bergh, Pengfei Yan*, Corsin Battaglia, Torsten Brezesinski and Yong Yang*

Dr. W. Zhao, R. Zhang, Dr. W. van den Bergh, Dr. T. Brezesinski

Institute of Nanotechnology, Karlsruhe Institute of Technology (KIT), Hermann-von-Helmholtz-Platz 1, 76344 Eggenstein-Leopoldshafen, Germany

E-mail: wengao.zhao@kit.edu

Dr. W. Zhao, M. Si, Dr. C. Battaglia

Materials for Energy Conversion, Empa - Swiss Federal Laboratories for Materials Science and Technology, 8600 Dübendorf, Switzerland

Dr. K. Wang, Z. Zhang, Prof. P. Yan

Beijing Key Laboratory of Microstructure and Properties of Solids, Faculty of Materials and Manufacturing, Beijing University of Technology, Beijing, China

Email: pfyan@bjut.edu.cn

F. Ren, Dr. X. Liu, Prof. Y. Yang

College of Chemistry and Chemical Engineering & College of Energy, Xiamen University, Xiamen, China

Email: [yyang@xmu.edu.cn](mailto:yayang@xmu.edu.cn)

Prof. X. Fan

School of Metallurgy and Environment, Central South University, Changsha, China

Email: fanxm@csu.edu.cn

X. Xu, Dr. Y. Liu

State Key Laboratory for Mechanical Behavior of Materials, Xi'an Jiaotong University, Xi'an, China

Dr. S. Xiong

Department of Physics, Chalmers University of Technology, 41296 Göteborg, Sweden

Abstract

Single-crystal $\text{LiNi}_{1-x-y}\text{Co}_x\text{Mn}_y\text{O}_2$ (SC-NCM, $x + y + z = 1$) cathodes are renowned for their high structural stability and reduced accumulation of adverse side products during long-term cycling. While advances have been made using SC-NCM cathode materials, careful studies of cathode degradation mechanisms are scarce. Herein, we employed quasi single-crystalline $\text{LiNi}_{0.65}\text{Co}_{0.15}\text{Mn}_{0.20}\text{O}_2$ (SC-NCM65) to test the relationship between cycling performance and material degradation for different charge cutoff potentials. The Li/SC-NCM65 cells showed $>77\%$ capacity retention below 4.6 V vs. Li^+/Li after 400 cycles and revealed a significant decay to 56% for 4.7 V cutoff. We demonstrate that the SC-NCM65 degradation is due to accumulation of rock-salt (NiO) species at the particle surface rather than intragranular cracking or side reactions with the electrolyte. The NiO-type layer formation is also responsible for the strongly increased impedance and transition-metal dissolution. Notably, the capacity loss is found to have a linear relationship with the thickness of the rock-salt surface layer. Density functional theory and COMSOL Multiphysics modelling analysis further indicate that the charge-transfer kinetics is decisive, as the lower lithium diffusivity of the NiO phase hinders charge transport from the surface to the bulk.

Keywords

Single crystal cathodes, structural stability, rock-salt formation, multiphysics analysis, transfer kinetics

Introduction

Single-crystalline $\text{LiNi}_{1-x-y}\text{Co}_x\text{Mn}_y\text{O}_2$ (SC-NCM, $x + y + z = 1$) cathode materials have garnered attention due to reports of greater stability owing to mitigation of particle fracture^[1]. In comparison, polycrystalline $\text{LiNi}_{1-x-y}\text{Co}_x\text{Mn}_y\text{O}_2$ (PC-NCM, $x + y + z = 1$) cathodes suffer from intergranular cracking under high-voltage operation and/or during long-term cycling. The reason is that the primary particles, which compose the larger secondary particles, experience competing anisotropic volume changes, leading to mechanical degradation and contact loss^[2]. In contrast, SC-NCM cathode materials consist of significantly larger crystallites (typically, $\geq 1 \mu\text{m}$) that are deagglomerated or whose secondary particles are made of several primary grains. This arrangement alleviates the mechanical degradation of the cathode by maintaining structural integrity upon cycling^[1e, 3]. In recent years, considerable progress has been made in improving the performance of SC-NCM cathodes including coating/doping strategies as well as mechanistic understanding of the electro-chemo-mechanical properties^[4]. Overall, lithium-ion cells using SC-NCM show promise for achieving better stability and higher volumetric energy densities than PC-NCM counterparts (for application in electric vehicles and portable devices), owing to the robust bulk structure and potentially greater tap density of (quasi) single-crystal battery materials^[1c, 1e, 5].

In general, quantifying the degradation of NCM is challenging because of the convolution of multiple parameters that may lead to capacity decay such as intra-/intergranular particle fracture, surface/subsurface phase transformation, cathode-electrolyte interphase (CEI) dissolution and reformation, and electrolyte decomposition.

SC-NCM particles with minimal grain boundaries represent an ideal model system to exclude degradation caused by intergranular cracking. Furthermore, accumulation of byproducts resulting from adverse side reactions can be mitigated, since the surface area is unlikely to undergo major changes during cycling^[4c, 6]. In addition, the interfacial chemistry can be tailored by varying the measurement conditions. Thus, SC-NCM cathode materials are suited for quantifying the degradation parameters by linking electrochemical performance and electrode/electrolyte interface evolution at the atomic level. While current research emphasizes the empirical improvements of SC-NCM through structural/surface engineering, the degradation parameters have not yet been examined thoroughly^[7].

Herein, we quantify the aforementioned parameters by studying cell cyclability and tracking the evolution of the surface composition and structure of SC-NCM ($\text{LiNi}_{0.65}\text{Co}_{0.15}\text{Mn}_{0.20}\text{O}_2$, referred to as SC-NCM65) particles. The cells reveal a similar stability for 4.4 to 4.6 V vs. Li^+/Li charge cutoff. However, severe capacity fading is observed for 4.7 V vs. Li^+/Li . Noteworthy, the degradation at 4.7 V operation is not a result of electrolyte decomposition, but instead due to decreasing Li^+ diffusivity with increasing rock-salt (NiO) surface formation. We demonstrate that the thickness of the disordered NiO-type layer on the surface of cycled SC-NCM65 displays a linear relation with its capacity loss. Density functional theory (DFT) confirms that the layered structure exhibits a lower energy barrier for lithium diffusion than the rock-salt phase, leading to faster transport kinetics. The NiO-type layer hinders Li-ion transport, as it possesses a much lower lithium diffusivity than the layered oxide structure^[8].

COMSOL Multiphysics simulation further corroborates that rock-salt formation accounts for the degradation due to sluggish Li^+ charge-transfer kinetics. Taken together, in the present work, we explore a (quasi) single-crystalline NCM cathode material that shows a promising performance, even in harsh conditions, and quantify the degradation by linking NiO-type surface formation, cutoff potential, and cycle number.

Results and Discussion

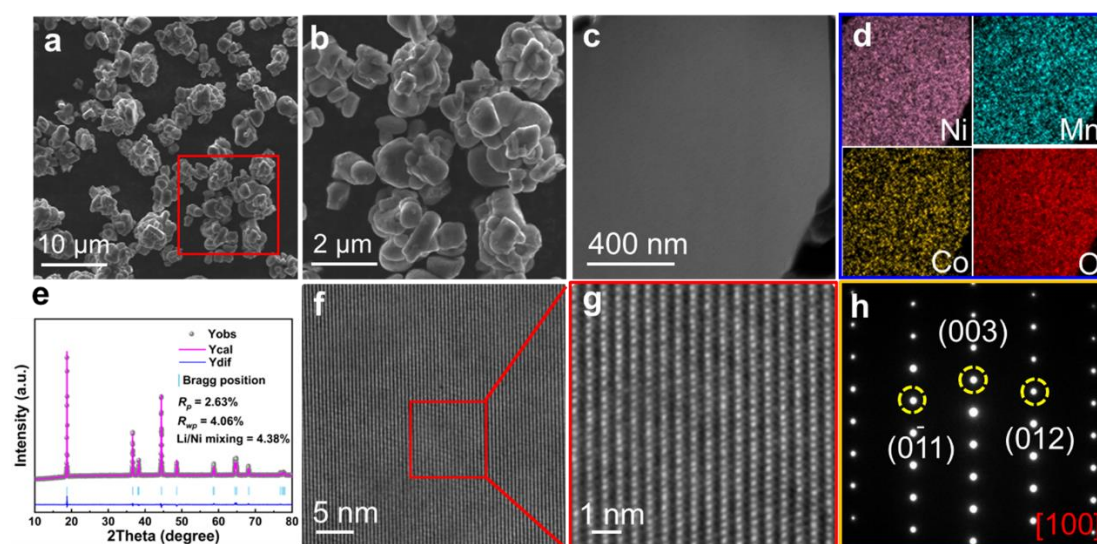


Figure 1. (a, b) SEM images, (c) low-magnification HAADF-STEM image and (d) corresponding EDS maps of Ni, Mn, Co, and O, (e) XRD pattern and Rietveld refinement profile, (f, g) high-magnification HAADF-STEM images, and (h) SEAD pattern of the SC-NCM65 particles.

The SC-NCM65 cathode material was synthesized by co-precipitation and subsequent calcination at 900 °C in O_2 atmosphere (see Experimental section for details). Scanning electron microscopy (SEM) images at different magnifications of the SC-NCM65 particles are presented in **Figure 1a, b**, revealing that they are composed of several primary particles of size 1-2 μm . From the cross-sectional high-angle annular

dark-field (HAADF)-scanning transmission electron microscopy (STEM) image in **Figure 1c** and the corresponding energy-dispersive X-ray spectroscopy (EDS) maps in **Figure 1d**, it is evident that the particles contain no internal porosity and Ni, Co, Mn, and O are uniformly distributed. The X-ray diffraction (XRD) pattern and Rietveld refinement profile in **Figure 1e** indicate a high degree of layering [(003)/(104) intensity ratio of 1.6 and clear splitting of the (006)/(102) and (018)/(110) reflections] with about 4.4% intermixing of Li^+ and Ni^{2+} in the structure (Ni_{Li} defects)^[9]. The refined lattice parameters are given in **Table S1** (see Supporting Information). The high ordering of the SC-NCM65 cathode material is also corroborated by high-magnification HAADF-STEM imaging (**Figure 1f, g**) and selected-area electron diffraction (SAED, **Figure 1h**).

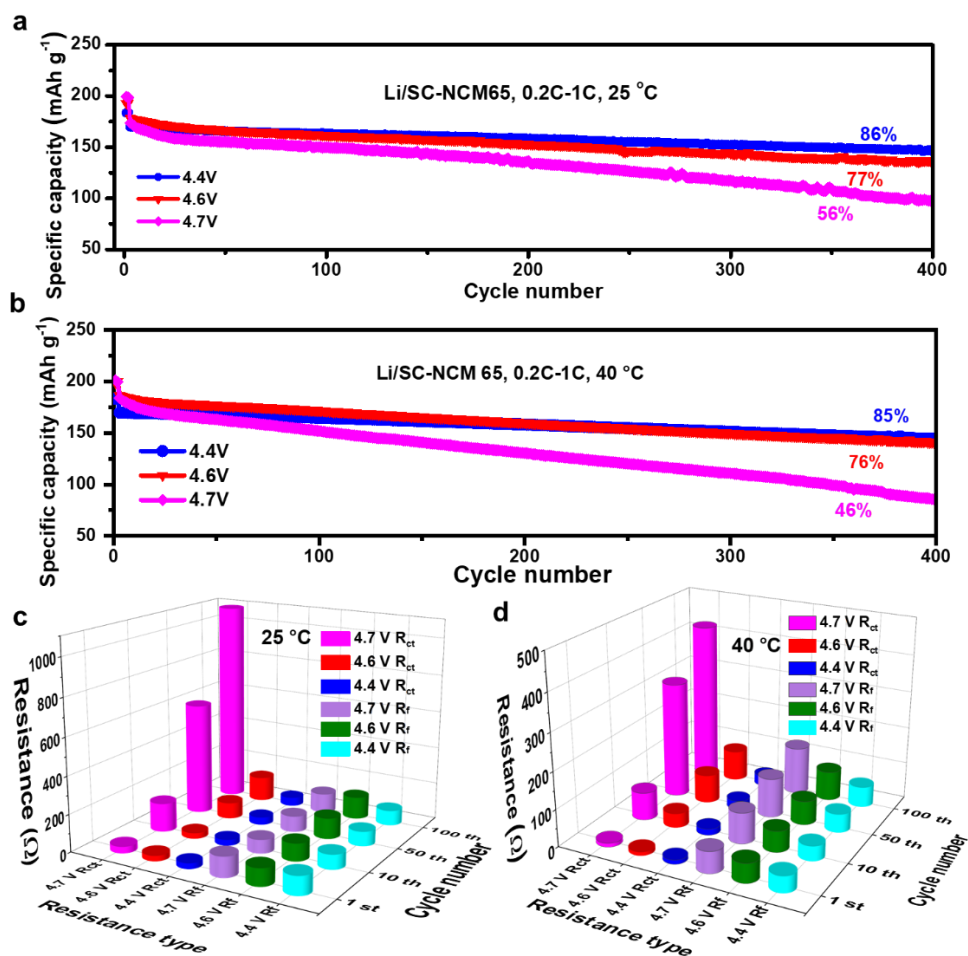


Figure 2. Long-term cycling performance of Li/SC-NCM65 cells at 25 °C (a) and 40 °C (b) and 0.2C charge/1C discharge for upper cutoff potentials of 4.4, 4.6, and 4.7 V vs. Li⁺/Li. The first two cycles were performed at 0.1C rate. Corresponding electrochemical impedance data for the 1st, 10th, 50th, and 100th cycle is shown in (c) and (d).

Figure 2 shows the discharge capacity comparison of SC-NCM65 in half cells for different upper cutoff potentials of 4.4, 4.6, and 4.7 V vs. Li⁺/Li at 25 and 40 °C. All cells underwent two formation cycles at 0.1C rate (1C = 180 mA g⁻¹) followed by cycling at 0.2C charge and 1C discharge. It is worth mentioning that the slow-charge/fast-discharge test protocol helps to exclude the Li metal anode instability maximumly and mainly assesses the cycling stability of cathodes^[10]. At 25 °C (**Figure**

2a), 86% of the specific capacity was retained for 4.4 V charge cutoff after 400 cycles and 77% for 4.6 V. However, the capacity retention decreased considerably to 56% with cycling in the potential range 2.7-4.7 V. At 40 °C (**Figure 2b**), the cells showed capacity retentions of 85, 76, and 46% for 4.4, 4.6, and 4.7 V, respectively. The stability is comparable at charge cutoff voltages of 4.4V and 4.6V with that achieved at 25 °C, while the cell delivers lower cyclability at 4.7V operation due to slightly severe electrode/electrolyte interface side reactions. The corresponding charge/discharge curves are shown in **Figure S1a-f**, revealing increasing polarization with increasing cutoff potential, in line with expectations. At 60 °C, the cells showed capacity retentions of only 75, 73, and 37% after 300 cycles (**Figure S2**). The faster capacity decay observed at 40 and 60 °C is presumably a result of the lower (electrode/electrolyte) interface stability^[11].

Electrochemical impedance spectroscopy (EIS) measurements provide insights into the state of health by monitoring the interphase resistance (R_f) and charge-transfer resistance (R_{ct})^[12]. **Figure S3a-f** shows Nyquist plots of the electrochemical impedance of Li/SC-NCM65 cells at 25 and 40 °C for the 1st, 10th, 50th, and 100th cycle. At 25 °C, the R_f was found to either remain constant or decrease initially and then to increase after about 10 cycles. However, the changes in R_f were relatively minor. The R_{ct} increased after the first cycle irrespective of the upper cutoff potential, due to the fact that interfacial reactions are occurring during cycling. The total change in R_{ct} was much larger for 4.7 V than for 4.4 and 4.6 V, as the harsh operating conditions induce unfavorable phase transformations in the cathode, thereby hindering lithium transport

and increasing cell polarization^[13]. Both the R_f and R_{ct} were smaller at 40 °C, since the elevated temperature results in faster kinetics. Nevertheless, it should be noted that the cells also showed a strong increase in R_{ct} with increasing cutoff potential, confirming that high-voltage operation negatively affects performance by altering the surface structure and composition of the SC-NCM65. Extracted resistances from fitting are given in **Tables S2** and **S3** and are summarized in **Figure 2c, d**, clearly showing the increase in R_{ct} with cycling, especially for the 4.7 V charge cutoff.

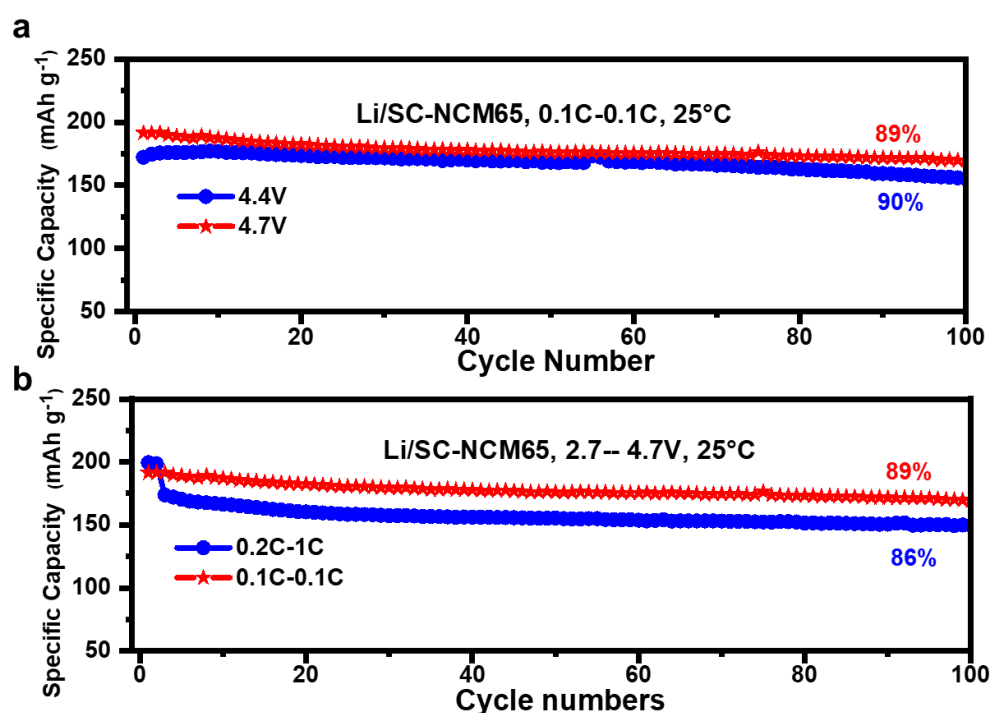


Figure 3. (a) Cycling performance of Li/SC-NCM65 cells at 25 °C and 0.1C charge/0.1C discharge for upper cutoff potentials of 4.4 and 4.7 V vs. Li⁺/Li. (b) Comparison of cyclability at 0.1C charge/0.1C discharge and 0.2C charge/1C discharge for 4.7 V charge cutoff.

As is evident from **Figure 2**, the cycling stability is inferior when charging the cells to 4.7 V. The general opinion is that electrolyte decomposition is one of the major reasons for the degradation under high-voltage operation^[14]. To confirm or disprove

this hypothesis, the cells were tested at 0.1C charge/0.1C discharge with upper cutoff potentials of 4.4 and 4.7 V (**Figure 3a**). Interestingly, the discharge capacity retention after 100 cycles was similar, with 90% for 4.4 V and 89% for 4.7 V. **Figure 3b** shows a comparison of the cycling performance in the potential range of 2.7-4.7 V for 0.1C charge/0.1C discharge and 0.2C charge/1C discharge. The cells delivered larger specific capacities at the lower C-rate and revealed a better capacity retention after 100 cycles, even though they might suffer from more severe electrolyte decomposition because of the longer charging time at high potentials (0.1 C vs. 0.2 C). Thus, it appears that electrolyte instability is not the single most critical problem that negatively affects cycling performance of the Li/SC-NCM65 cells.

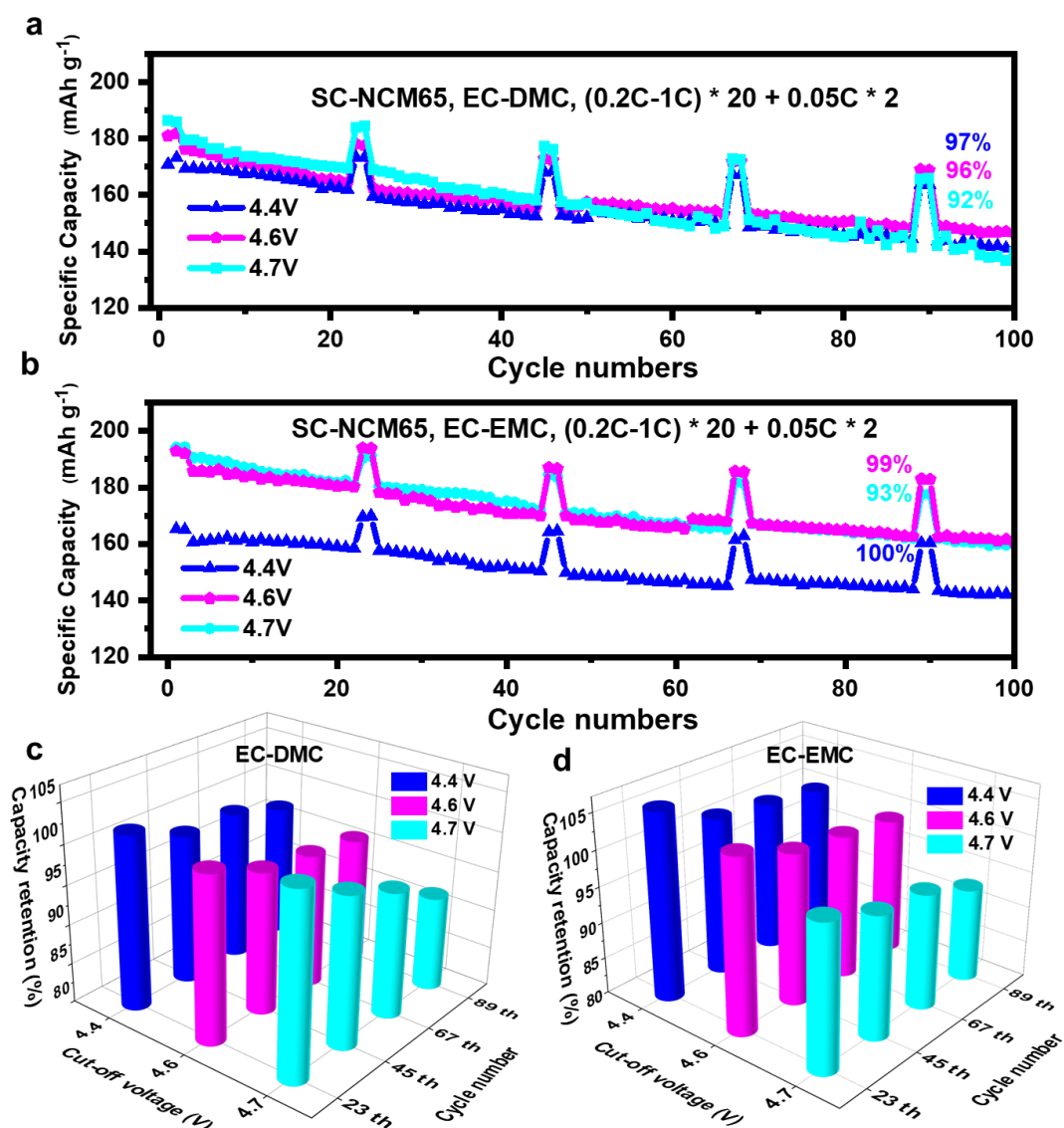


Figure 4. Cycling performance of Li/SC-NCM65 cells with EC-DMC (a) and EC-EMC (b) electrolyte at 25 °C and 0.2C charge/1C discharge for upper cutoff potentials of 4.4, 4.6, and 4.7 V vs. Li⁺/Li. The cells were tested for two cycles at 0.05C charge/0.05C discharge every 20 cycles, and the first two cycles were performed at 0.1C rate.

To gain more insights into the factors that determine the stability of the Li/SC-NCM65 cells, their cyclability at 0.2C charge/1C discharge with low C-rate testing (0.05C) every 20 cycles was examined for the different upper cutoff potentials (**Figure 4**). All cells showed a rather linear discharge capacity decay over the first 100 cycles. After 89 cycles, 97, 96, and 92% of the initial specific capacity was recovered for 4.4,

4.6, and 4.7 V charge cutoff, respectively, see **Figure 4a, c** and **Table S4**. From this data, it is clear that the Li^+ transfer kinetics strongly affects the overall performance, as the slow charge-discharge leads to a more homogeneous Li^+ extraction/distribution in the cathode's bulk structure while the fast charging-discharging subjects to the defects or non-uniform Li^+ mobility process^[15]. The higher capacity loss for 4.7 V is presumably a result of surface rock-salt (NiO) formation (surface damage) and/or bulk structural instabilities upon high-voltage operation^[1e, 4d, 16]. However, differences in electrolyte decomposition cannot be ruled out. In addition to the ethylene carbonate (EC)-dimethyl carbonate (DMC) electrolyte, the cells were also tested using EC-ethyl methyl carbonate (EMC) under the same cycling conditions. Notably, they showed similar trends to the cells with EC-DMC electrolyte, see **Figure 4b, d** and **Table S5**, thus supporting that the (interfacial/bulk) transport properties determine the reversible capacity in case of the Li/SC-NCM65 cells.

To see whether or not the CEI formed on the cycled cathodes (400 cycles at 25 °C and 0.2C charge/1C discharge) hinders lithium transport by passivating the cathode/electrolyte interface, it was probed using X-ray photoelectron spectroscopy (XPS). Peaks characteristic of C-C, C-O, C=O, and OCO_2 bonds were observed in the C1s spectra (**Figure S4a**), with no major differences in intensities and area ratios between 4.4 and 4.6 V charge cutoff. $\text{Li}_x\text{PO}_y\text{F}_z$ and LiF formation were found to decrease and increase respectively with increasing cutoff potential (see F1s spectra in **Figure S4b**) with significant changes between 4.4 and 4.6/4.7 V. With respect to R_{ct} trends (**Figure 2c**), it is unlikely that either of the changes with surface $\text{Li}_x\text{PO}_y\text{F}_z$ and

LiF account for the increased resistance. The O1s data also revealed an increase in carbonate peak intensity from 4.4 to 4.7 V (**Figure S4c**), indicating some differences in electrolyte decomposition during cycling. However, the intensity of the M-O (lattice oxygen) peak did not change much with cutoff potential (from 4.6 to 4.7 V), which suggests that high-voltage operation does not necessarily lead to formation of a thicker CEI. The results obtained from quantitative XPS analysis are given in **Table S6**. Overall, the relatively similar composition and thickness of the CEI on the free surface of the cycled SC-NCM65 particles demonstrates that it only accounts to some degree for the differences seen in the cyclability between 4.4, 4.6, and 4.7 charge cutoff.

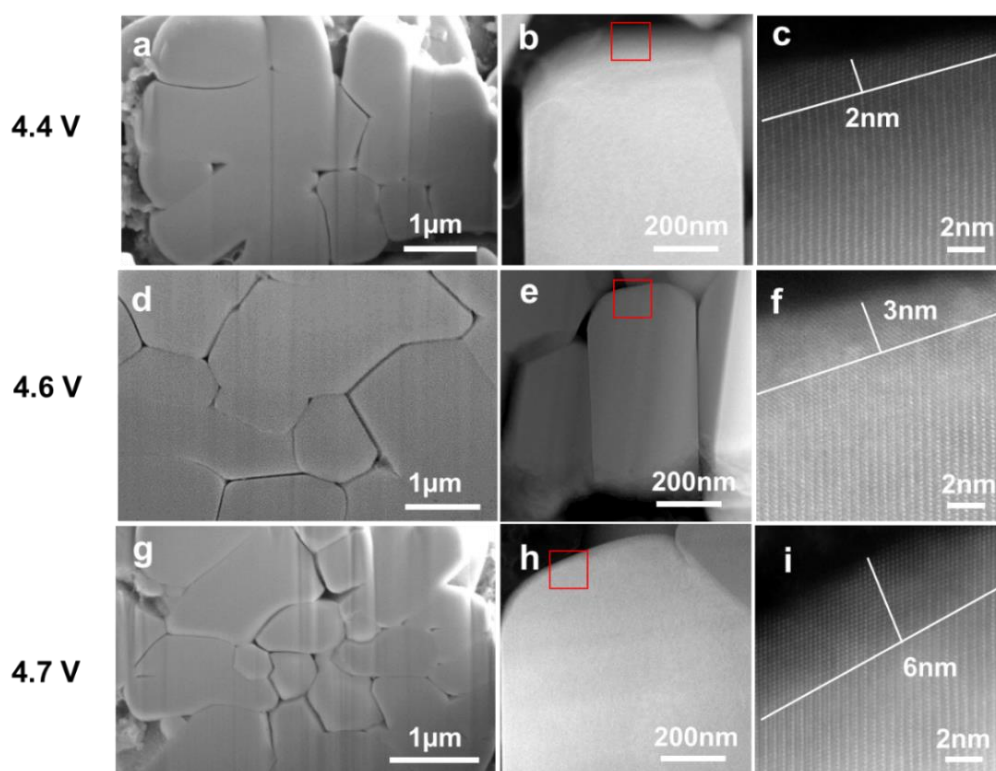


Figure 5. Cross-sectional SEM images and HAADF-STEM images at different magnifications of the SC-NCM65 particles after 400 cycles at 25 °C and 0.2C charge/1C discharge: 4.4 V (a-c), 4.6 V (d-f), and 4.7 V vs. Li⁺/Li (g-i).

Post-mortem analysis was also conducted on the cycled cathodes to examine the morphology and surface structure of the SC-NCM65 particles. To this end, the harvested electrodes were soaked and rinsed with DMC to remove surface contaminants and then dried in an Ar-filled glovebox. **Figure 5a, d, g** shows cross-sectional SEM images indicating minor crack formation along the grain boundaries, meaning the particle integrity was well maintained after cycling. Intergranular cracking has been shown to be one of the reasons for impedance buildup and capacity fading of conventional (polycrystalline) layered oxide cathodes. However, single crystal or quasi single-crystalline NCM materials have a robust bulk structure and thus show little susceptibility to (intragranular) cracking under high-voltage operation or during long-term cycling^[1e, 4c, 5a, 16-17]. It should be noted that several particles from the cycled cathodes were analyzed, see **Figure S5**, with all of them showing some, but mostly minor cracking. Because the long-term cycling stability was found to decrease with increasing charge cutoff potential and there were no major differences in the degree of SC-NCM65 particle fracture, inter-/intragranular cracking is likely not the root cause for the observed capacity degradation.

Figure 5b, e, h shows low-magnification HAADF-STEM images of the cycled SC-NCM65 particles, with the red squares denoting the areas probed in **Figure 5c, f, i**. High-magnification imaging revealed the presence of a disordered rock-salt surface layer of average thickness 2 nm for 4.4 V, 3 nm for 4.6 V, and 6 nm for 4.7 V. Note that the NiO-type phase formation is associated with lattice oxygen loss and Li⁺/Ni²⁺ cation mixing during cycling^[18]. The thickness of the surface layer in different areas of the

cathode particles is indicated in the images shown in **Figure S6**. The above data demonstrate that there is a link between surface rock-salt formation and Li^+ charge-transfer kinetics, both of which depend directly or indirectly on the charge cutoff potential^[19]. Additionally, transition-metal leaching from the SC-NCM65 was found to be more pronounced when cycling the cells in the potential range 2.7-4.7 V, see **Table S7**. This is probably also related (at least in part) to the structural evolution of the cathode particles during cycling. From the XPS and microscopy results, it can be concluded that the surface phase transformation has a strong effect on the long-term cycling performance of the SC-NCM65 cathodes.

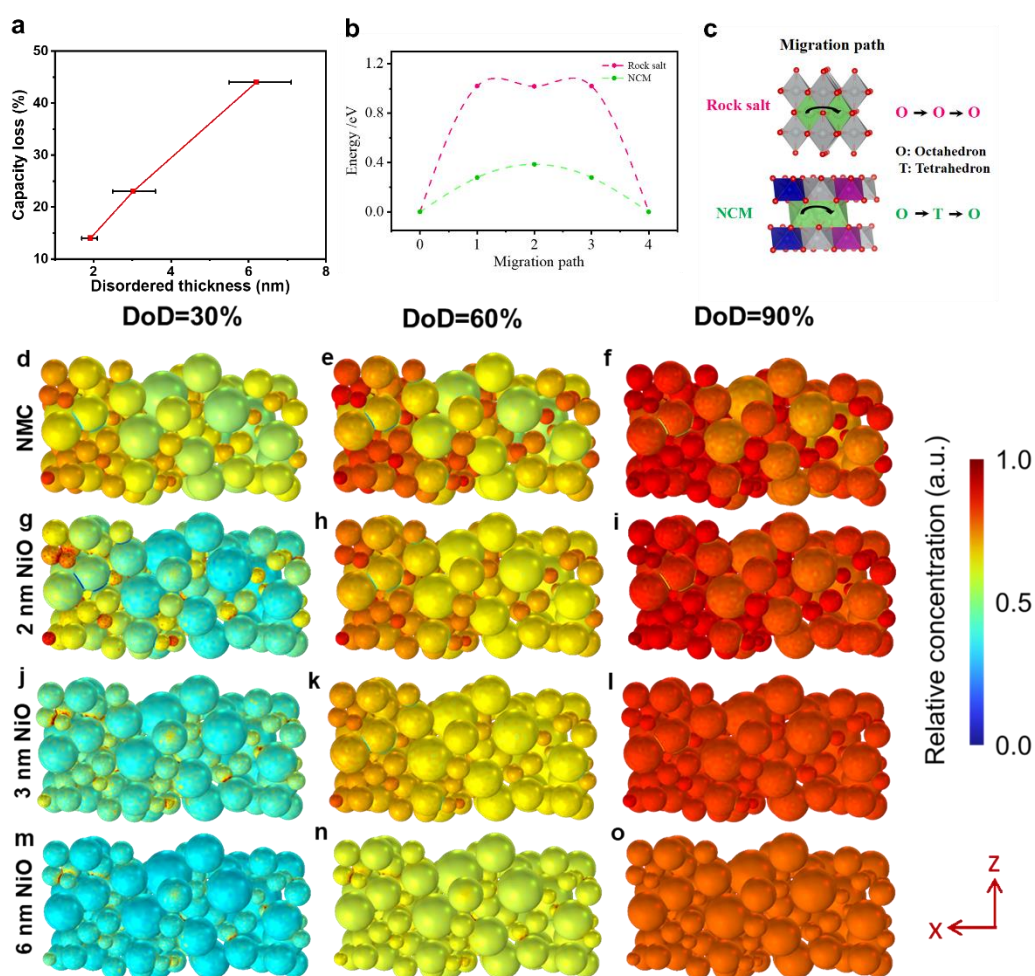


Figure 6. (a) Correlation between relative capacity loss and thickness of the rock-salt surface layer formed on the SC-NCM65 particles during cycling. (b) Static energy

distribution along the migration path from DFT. (c) Lithium diffusion pathways in ordered NCM and disordered NiO. Lithium concentration distribution on the surface of the SC-NCM65 particles. The thickness of the rock-salt layer is set to 0 nm (d-f), 2 nm (g-i), 3 nm (j-l), and 6 nm (m-o), and the depth of discharge (DoD) varies from 30 to 90%.

Figure 6 examines the correlation between cycling performance and surface phase transformation by quantifying relative capacity loss and rock-salt formation after 400 cycles for charge cutoff potentials of 4.4, 4.6, and 4.7 V. As can be seen from **Figure 6a**, there is a linear relationship between relative capacity loss and thickness of the NiO-type layer, which provides evidence that primarily rock-salt surface degradation determines the cycling performance. **Figure 6b** compares the energy barrier for lithium diffusion for ordered NCM and disordered NiO. In fact, the effective diffusion barrier for NiO is much larger than that of NCM (0.35 eV vs 1.02 eV), indicating that the Li⁺ diffusion kinetics is different for both phases [considering the equation relating activation energy to lithium diffusion: $D_{Li} = \frac{1}{2} a^2 \nu \exp(-E_a/kT)$]^[20]. The lithium diffusion pathways are shown in **Figure 6c**. In NCM, Li⁺ ions tend to diffuse from one octahedral site to the next by hopping through an intermediate tetrahedral site (depending on the state of charge), while in disordered NiO there is an intermediate distorted octahedral site.

Because the lithium transport is very complex in general, COMSOL Multiphysics was used to simulate the lithium concentration distribution considering both the thickness of the rock-salt surface layer and the particle size^[8]. The intercalation of Li⁺ ions into single cathode particles is visualized for different depth of discharge (DoD) in

Figure S7. As expected, the Li-ion concentration in a single particle gradually increased upon discharge, and all samples were found to have a gradient distribution (from the surface to the particle center). However, the Li-ion concentration in the particle strongly decreased with increasing thickness of the NiO-type surface layer. For achieving a realistic simulation and building the geometrical model of the cathode, the particle size distribution, electrode thickness, and surface/bulk ionic conductivity were considered (**Figure S8**). The Li-ion concentration distribution on the surface of the SC-NCM65 particles is shown in **Figure 6d-o**. Again, the concentration clearly increased with increasing DoD, similar to the single particle case. However, it decreased notably for rock-salt surface layer thicknesses > 2 nm, indicating that sluggish charge transfer adversely affects the intercalation dynamics, ultimately leading to capacity decay. Apart from that, the lithium concentration (from the electrode surface to the current collector) was found to be more uniform for particles having a rock-salt surface layer, suggesting the potential for recovering the capacity at low current densities. This finding agrees well with the cycling data shown in **Figure 4**. The Li-ion concentration field (cross section) in the SC-NCM65 particles is shown in **Figure S9**, corroborating the above results. Overall, the COMSOL Multiphysics simulation confirms that the lithium transport kinetics determines the reversible capacity of the SC-NCM65 cathode.

Conclusions

In the present work, we have electrochemically tested a (quasi) SC-NCM65 cathode material in Li-ion cells with the objective to quantify the degradation parameters by

correlating capacity loss and disordered rock-salt surface formation (after ruling out particle fracture and electrolyte decomposition as root causes for the capacity fading). With increasing charge cutoff potential, the cells were found to show accelerated degradation (lower capacity retention) and increased polarization due to formation of a relatively thick NiO-type layer on the surface of the SC-NCM65 particles. DFT calculations revealed that the disordered rock-salt NiO layer exhibits a lower effective energy barrier for lithium diffusion than the layered NCM phase. COMSOL Multiphysics simulation further confirmed that the lithium transport kinetics is negatively affected by the rock-salt surface formation.

Taken together, we have quantified, to our knowledge for the first time, the degradation parameters for a SC-NCM material, which might help develop single crystal cathodes with enhanced cycling performance and stability under high-voltage operation.

Acknowledgements

This work received financial support from the National Natural Science Foundation of China (no. 12104024, 52204328, 22261160570), China National Postdoctoral Program for Innovative Talents (BX2021024), and Chinese Postdoctoral Science Foundation (2020M680273, 2022M713547).

Conflict of Interest

The authors declare no conflict of interest.

Data Availability Statement

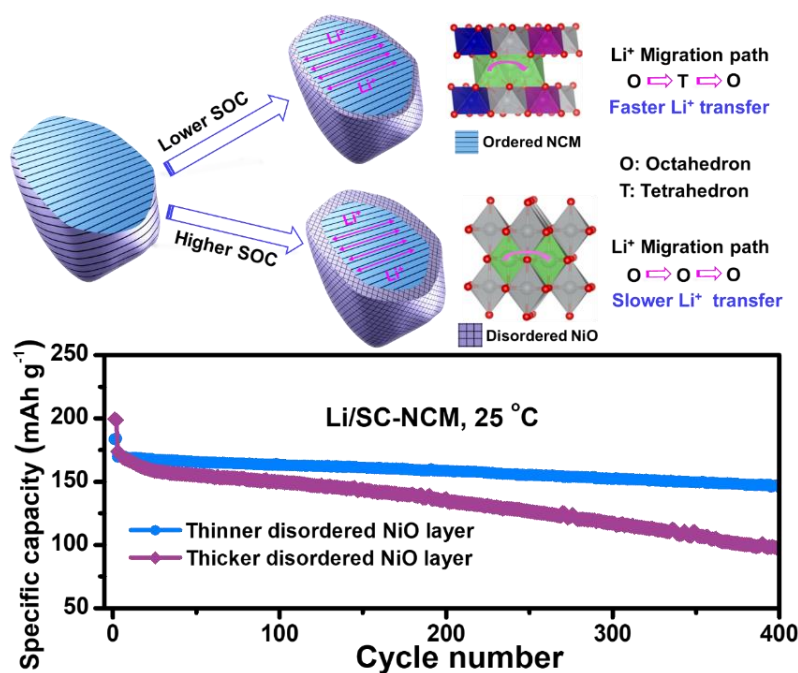
The data that support the findings of this study are available from the corresponding author upon reasonable request.

References

- [1] a) H. Li, J. Li, X. Ma, J. R. Dahn, *J. Electrochem. Soc.* **2018**, *165*, A1038-A1045; b) Y. Han, Y. Lei, J. Ni, Y. Zhang, Z. Geng, P. Ming, C. Zhang, X. Tian, J. L. Shi, Y. G. Guo, Q. Xiao, *Small* **2022**, 2107048; c) X. Fan, X. Ou, W. Zhao, Y. Liu, B. Zhang, J. Zhang, L. Zou, L. Seidl, Y. Li, G. Hu, C. Battaglia, Y. Yang, *Nat. commun.* **2021**, *12*, 5320; d) W. Bao, G. Qian, L. Zhao, Y. Yu, L. Su, X. Cai, H. Zhao, Y. Zuo, Y. Zhang, H. Li, Z. Peng, L. Li, J. Xie, *Nano Lett.* **2020**, *20*, 8832-8840; e) W. Zhao, L. Zou, L. Zhang, X. Fan, H. Zhang, F. Pagani, E. Brack, L. Seidl, X. Ou, K. Egorov, X. Guo, G. Hu, S. Trabesinger, C. Wang, C. Battaglia, *Small* **2022**, *18*, 2107357.
- [2] a) H.-H. Ryu, K.-J. Park, C. S. Yoon, Y.-K. Sun, *Chemistry of Materials* **2018**, *30*, 1155-1163; b) P. Yan, J. Zheng, J. Liu, B. Wang, X. Cheng, Y. Zhang, X. Sun, C. Wang, J.-G. Zhang, *Nat. Energy* **2018**, *3*, 600-605.
- [3] a) J. Langdon, A. Manthiram, *Energy Stor. Mater.* **2021**, *37*, 143-160; b) L. Ni, S. Zhang, A. Di, W. Deng, G. Zou, H. Hou, X. Ji, *Adv. Energy Mater.* **2022**, *12*, 2201510.
- [4] a) J. Li, H. Li, W. Stone, S. Glazier, J. R. Dahn, *J. Electrochem. Soc.* **2018**, *165*, A626-A635; b) Y. Lu, T. Zhu, E. McShane, B. D. McCloskey, G. Chen, *Small* **2022**, *18*, 2105833; c) X. Fan, G. Hu, B. Zhang, X. Ou, J. Zhang, W. Zhao, H. Jia, L. Zou, P. Li, Y. Yang, *Nano Energy* **2020**, *70*, 104450; d) F. Zhang, S. Lou, S. Li, Z. Yu, Q. Liu, A. Dai, C. Cao, M. F. Toney, M. Ge, X. Xiao, W. K. Lee, Y. Yao, J. Deng, T. Liu, Y. Tang, G. Yin, J. Lu, D. Su, J. Wang, *Nat. commun.* **2020**, *11*, 3050; e) X. Ou, T. Liu, W. Zhong, X. Fan, X. Guo, X. Huang, L. Cao, J. Hu, B. Zhang, Y. S. Chu, G. Hu, Z. Lin, M. Dahbi, J. Alami, K. Amine, C. Yang, J. Lu, *Nat. commun.* **2022**, *13*, 2319.
- [5] a) L. Ni, R. Guo, S. Fang, J. Chen, J. Gao, Y. Mei, S. Zhang, W. Deng, G. Zou, H. Hou, X. Ji, *eScience* **2022**, *2*, 116-124; b) J. Li, H. Li, W. Stone, R. Weber, S. Hy, J. R. Dahn, *J. Electrochem. Soc.* **2017**, *164*, A3529-A3537.
- [6] a) H. Cha, J. Kim, H. Lee, N. Kim, J. Hwang, J. Sung, M. Yoon, K. Kim, J. Cho, *Adv. Mater.* **2020**, *32*, 2003040; b) W. Liu, P. Oh, X. Liu, M. J. Lee, W. Cho, S. Chae, Y. Kim, J. Cho, *Angew. Chem. Int. Ed.* **2015**, *54*, 4440-4457.
- [7] a) X. Kong, Y. Zhang, S. Peng, J. Zeng, J. Zhao, *ACS Sustain. Chem. Eng.* **2020**, *8*, 14938-14948; b) X. Fan, Y. Liu, X. Ou, J. Zhang, B. Zhang, D. Wang, G. Hu, *Chem. Eng. J.* **2020**, *393*, 124709.
- [8] a) S. Wang, M. Yan, Y. Li, C. Vinado, J. Yang, *J. Power Sources* **2018**, *393*, 75-82; b) D. J. S. A. Audeh, J. B. Alcázar, C. V. Barbosa, N. L. V. Carreño, C. A. O. Avellaneda, A. J. Pawlicka, E. Raphael, *Polímeros Ciência e Tecnologia* **2014**, *24*, 8-12.
- [9] a) J. Zheng, P. Yan, L. Estevez, C. Wang, J.-G. Zhang, *Nano Energy* **2018**, *49*, 538-548; b) W. Zhao, H. Jia, J. Zheng, D. Wang, J. Song, R. Liu, C. Hong, W. Xu, Y. Yang, J. Xiao, C.-M. Wang, and J.-G. Zhang, *ACS Appl. Energy Mater.* **2020**, *3*, 3369-3377.
- [10] a) D. Lu, Y. Shao, T. Lozano, W. Bennett, G. Graff, B. Polzin, J. Zhang, M. Engelhard, N. Saenz, W. Henderson, P. Bhattacharya, J. Liu, J. Xiao, *Adv. Energy. Mater.* **2015**, *5*, 1400993; b) J. Zheng, P. Yan, D. Mei, M. Engelhard, S. Cartmell, B. Polzin, C. Wang, J.-G. Zhang, W. Xu, **2016**, *6*, 1502151
- [11] a) H. Kim, M. G. Kim, H. Y. Jeong, H. Nam, J. Cho, *Nano Lett.* **2015**, *15*, 2111-2119; b) S. S. Zhang, *Energy Stor. Mater.* **2020**, *24*, 247-254; c) S. Yang, Q. Fan, Z. Shi, L. Liu, J. Liu, X.

- Ke, J. Liu, C. Hong, Y. Yang, Z. Guo, *ACS Appl. Mater. Inter.* **2019**, *11*, 36742-36750.
- [12] a) P. Jones, U. Stimming, A. Lee, *Nat. commun.* **2022**, *13*, 4806; b) C. Zheng, S. Tang, F. Wen, J. Peng, W. Yang, Z. Lv, Y. Wu, W. Tang, Z. Gong, Y. Yang, *Mater. Futures* **2022**, *1*, 045103; c) J. Teo., S. Florian, W. Felix, M. Yuan, P. Seyedhosein, S. Torsten, B. Matteo, J. Jürgen, B. Torsten, *Mater. Futures* **2022**, *1*, 015102.
- [13] a) S. Tan, Z. Shadike, J. Li, X. Wang, Y. Yang, R. Lin, A. Cresce, J. Hu, A. Hunt, I. Waluyo, L. Ma, F. Monaco, P. Cloetens, J. Xiao, Y. Liu, X.-Q. Yang, K. Xu, E. Hu, *Nat. Energy* **2022**, *7*, 484-494; b) H. Gao, P. Lamp, K. Amine, and Z. Chen, *ACS Appl. Mater. Inter.* **2017**, *9*, 44542-44549.
- [14] a) S. K. Heiskanen, N. Laszczynski, B. L. Lucht, *J. Electrochem. Soc.* **2020**, *167*, 100519; b) N. Laszczynski, S. Solchenbach, H. A. Gasteiger, B. L. Lucht, *J. Electrochem. Soc.* **2019**, *166*, A1853-A1859.
- [15] a) S. Schindler, M. Bauer, M. Petzl, M-A. Danzer, *J. Power Sources* **2016**, *304*, 170–180; b) B. Epping, B. Rumberg, H. Jahnke, I. Stradtman, A. Kwade, *J. Energy Storage* **2019**, *22*, 249–256; c) X. Liu, C-B. Arnold, *J. Electrochem. Soc.* **2020**, *167*, 130519
- [16] H.-J. Guo, Y. , Y. Z. , G-X. Liu, Y-X. Song, J. Wan,, Y.-G. Guo. K-C Jiang, X. Sun, and R. Wen, *Angew. Chem. Int. Ed.* **2022**. *61*, 202211626
- [17] X. Fan, Y. D. Huang, H. X. Wei, L. B. Tang, Z. J. He, C. Yan, J. Mao, K. H. Dai, J. C. Zheng, *Adv. Funct. Mater.* **2021**, *32*, 2109421.
- [18] L. Zou, Z. Liu, W. Zhao, H. Jia, J. Zheng, Y. Yang, G. Wang, J.-G. Zhang, C. Wang, *Chem. Mater.* **2018**, *30*, 7016-7026.
- [19] a) L. Zou, W. Zhao, Z. Liu, H. Jia, J. Zheng, G. Wang, Y. Yang, J.-G. Zhang, C. Wang, *ACS Energy Lett.* **2018**, *3*, 2433-2440; b) L. Zou, W. Zhao, H. Jia, J. Zheng, L. Li, D-P. Abraham, G. Chen, J.-G. Zhang. J- R. Croy, and C-M. Wang, *Chem. Mater.* **2020**, *32*, 2884-2892; c) J. Li, J. Wu, S. Li, G. Liu, Y. Cui, Z. Dong, H. Liu, X. Sun, *ChemSusChem* **2021**, *14*, 2721-2730; d) X. Zhang, L. Zou, Z. Cui, H. Jia, M-H. Engelhard, B- E. Matthews, Q. Xie, C-M. Wang, J.-G. Zhang, A. Manthiram, W. Xu, *Mater. Today* **2021**, *44*, 15-24; e) S. Jiao, X. Ren, R. Cao, M. H. Engelhard, Y. Liu, D. Hu, D. Mei, J. Zheng, W. Zhao, Q. Li, N. Liu, B. D. Adams, C. Ma, J. Liu, J.-G. Zhang, W. Xu, *Nat. Energy* **2018**, *3*, 739-746.
- [20] K. Tang, X. Yu, J. Sun, H. Li, X. Huang, *Electrochim. Acta* **2011**, *56*, 4869-4875.

Table of Contents



In this work, we demonstrate that the SC-NCM65 degradation is due to accumulation of rock-salt (NiO) species at the particle surface rather than intragranular cracking or side reactions with the electrolyte. Notably, the cycling stability shows an inverse relationship with the thickness of the rock-salt surface layer. Simulation analysis further indicate that the slower Li⁺ diffusivity of NiO mainly accounts for the cycling decay of cathode.

Socia media promotion

Wengao Zhao Twitter account: Jacky-Gao001

Torsten Brezesinski Twitter account: Tbrezesinski

Corsin Battaglia Twitter account: BattagliaCorsin

Wengao Zhao (first author), Dr. Torsten Brezesinski, Prof. Pengfei Yan, Dr. Shizhao Xiong, Prof. Corsin Battaglia, and Prof. Yong Yang (last author) should be included on the Twitter post.